COMPUTER-AIDED DESIGN & APPLICATIONS, 2018
VOL. 15, NO. 5, 720–733
https://doi.org/10.1080/16864360.2018.1441239

Cylinder-based simultaneous registration and model fitting of laser-scanned point clouds for accurate as-built modeling of piping system

Ryota Moritani [a], Satoshi Kanai [a], Hiroaki Date [a], Masahiro Watanabe [b], Takahiro Nakano [b] and Yuta Yamauchi [b]

[a]Hokkaido University, Japan; [b]Hitachi, Ltd., Japan

ABSTRACT

In this study, a novel algorithm for cylinder-based registration and model fitting of laser-scanned point clouds was proposed. The algorithm was designed specifically for as-built modeling of a plant piping system. In contrast with Iterative Closest Point (ICP)-based methods, fine registration and model fitting were performed simultaneously, by solving a single nonlinear constraint equation. This prevented alignment error arising in registration from propagating to model fitting. Coarse registration was automated by identifying cylindrical surfaces and by finding matches among their cylinder axes using a random sample consensus (RANSAC) method. The accuracy and robustness of the proposed algorithm was first confirmed using scan simulations. It performed well even when there was zero overlap between scans, and was demonstrated to achieve better modeling accuracy than ICP-based methods. The algorithm was then applied to point clouds scanned from a real plant, with successful results. The proposed algorithm achieves as-built modeling accuracies that would be fully acceptable when conducting renovation work on existing piping systems.

KEYWORDS

Laser scanning; as-built modeling; registration; point clouds; piping system; terrestrial laser scanner; plant engineering

1. Introduction

As product life cycles shorten, the frequency with which chemical, petroleum, and gas plants require updating has been increasing. This creates a growing need to improve the efficiency of renovation work. The same is happening in the heating, ventilation, and air-conditioning (HVAC) systems of buildings. A critical factor in the efficient renovation works is how to identify the exact locations of existing facilities in surveys and how to design new facilities to fit perfectly with them, since the previous drawings only give two-dimensional information and often vary with their "as-built" or "as-is" status. Complex and tangled piping systems occupy large areas of these plants, so that capturing the as-built status of the piping system is crucial when planning a renovation.

This has encouraged the application of 3D laser scanning and as-built CAD modeling to complex piping systems. In as-built modeling, multiple partially scanned point clouds, largely composed of cylindrical pipes, are captured from different viewpoints using a terrestrial laser scanner (TLS). A registration process then aligns these point clouds into a consistent coordinate system. Parameters such as the position, orientation, and diameter of the pipes are then estimated by fitting mathematical models of cylinders to the registered point clouds. Both the registration process and model fitting must be highly accurate to derive an as-built model that is suitable for use in renovation. This means, for example, that the positional error in alignment of the centerlines of the new pipe and existing pipe should be less than 5 mm at the end faces.

The registration process of the TLS point clouds consists of coarse and fine registration. Coarse registration is used to identify the approximate alignment of the scans. Fine registration then minimizes the distance between corresponding points at the overlap between adjacent scans. A range of automatic coarse registration methods have been reported [21]. In contrast, the Iterative Closest Point (ICP) algorithm is normally used in fine registration [3]. However, when the overlap between scans is very small or absent, the ICP algorithm fails. Moreover, even when overlap is achieved, the ICP leaves non-negligible alignment errors between scans, ultimately degrading the accuracy of the cylinder model fitting. This is shown in Fig. 1(a).

CONTACT Ryota Moritani r_moritani@sdm.ssi.ist.hokudai.ac.jp; Satoshi Kanai kanai@ssi.ist.hokudai.ac.jp; Hiroaki Date hdate@ssi.ist.hokudai.ac.jp; Masahiro Watanabe masahiro.watanabe.ub@hitachi.com; Takahiro Nakano takahiro.nakano.tz@hitachi.com; Yuta Yamauchi yuta.yamauchi.kj@hitachi.com

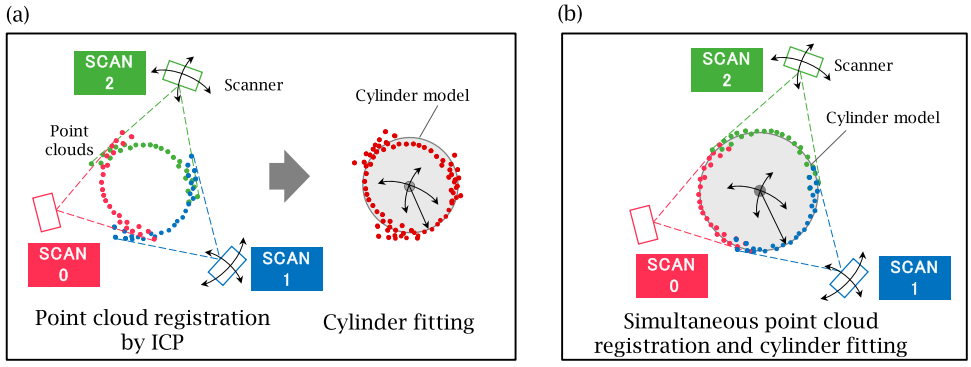

Figure 1. Differences in registration and model fitting process of scanned points of piping system: (a) Conventional ICP-based registration and model fitting process, and (b) Proposed registration and model fitting process.

To address this, we proposed a new algorithm for cylinder-based registration and model fitting of laser-scanned point clouds. The algorithm was specifically designed for as-built modeling of the pipes found in plants. As shown in Fig. 1(b)., our algorithm differs from the conventional ICP-based method, as it simultaneously solves fine registration and model fitting by expressing them as a single nonlinear constraint equation. This removes the alignment error that arises in registration from propagation to model fitting. The algorithm works even when there is zero overlap between scans, and achieves a more accurate registration and fitting than the ICP-based method. Coarse registration is automated by identifying partial cylindrical surfaces in each scan as geometric features for use in alignment, then finding an appropriate match among their cylinder axes using RANSAC [6]. Through scan simulations, the registration and modeling accuracy of the proposed algorithm was compared with that of a conventional ICP-based method, and the superiority of the proposed algorithm was demonstrated. Application to real point clouds scanned from a HVAC plant confirmed the practicality of the proposed algorithm.

The rest of this paper is organized as follows. The previous literature on registration methods and the problems with them are discussed in Section 2. Our cylinder-based coarse registration algorithm is described in Section 3, and the fine registration algorithm in Section 4. Measurement error modeling and our scan simulation software are introduced in Section 5. Section 6 presents the results of a comparison between our algorithm and an ICP-based algorithm, using both point clouds from a scan simulation and real point clouds captured from an HVAC plant.

2. Related work

Point cloud registration is an indispensable processing used for aligning multiple partial scans captured from different scanner positions, mapping them to consistent coordinates. Two types of registration method are used: marker-based and marker-less. Marker-based methods attach a set of artificial fiducial markers to the object surface, then identify an appropriate alignment among them. These methods afford high accuracy and robustness, and are widely used in laser-scanning applications. As the fiducial marker, small planar plates with black and white patterns or spheres [28] are generally used. However, marker installation is a dangerous and time-consuming process, especially when working high within a piping system. The accuracy of registration depends on the number of markers installed by the operator, and their placement.

Marker-less methods are used in both fine and coarse registration. The best-known fine registration algorithm is the ICP [3], in which the sum of the squared distances between the closest points in two scans are minimized in an iterative manner, to derive the best transformation for aligning them. Many variants of the ICP have been proposed [1], [11], [14], [16], [17]. Fine registration methods that minimize the sum of squares of the distances between surfaces in the point clouds have also been proposed [7], [9], and these are able to be solve all types of 3D surface correspondence.

However, these minimization-based fine registration methods depend on sufficient overlaps between two scans being present, and a good initial alignment between the two scans is essential for achieving convergence to a precise alignment. If the overlap between scans is small or absent, or the initial alignment includes some degree of deviation, false matches are created and the registration converges to an incorrect solution. This is often the case when a set of dense and tangled cylindrical pipes are scanned from a small number of positions. A second problem with these methods is that fine registration and model fitting are carried out separately. Even when an overlap between scans is available, the fine registration process leaves non-negligible alignment errors

among the scans. This degrades the accuracy of cylinder model fitting when conducting as-built modeling of piping systems.

Over recent years, many marker-less coarse registration methods for TLS point clouds have been proposed. These attempts to produce consistent initial alignments between different scans for fine registration. A range of geometric features are extracted from the scans and used to estimate the initial alignments, with only small deviations. The geometric features used for registration have included point, line, and plane features. Point features have included SIFT feature points in TLS reflectance images [26], DoG and 3D Harris key points [24], and fast point feature histograms [18]. Linear line features [2], [10], plane features [23], [15], and a combination of linear and plane features [20] have also been proposed. Other studies have made use of semantically-enriched features such as window, roof, and wall attributes [22], and ground feature points with artificial object attributes [27].

However, these methods have been designed to achieve a coarse alignment between scans, and cannot necessarily achieve the registration accuracy required for the model fitting of a piping system. Moreover, although cylindrical surfaces constitute a vast majority of the surfaces in the scanned point clouds of plant piping systems, the cylindrical features have not been efficiently used in these coarse registrations.

3. Cylinder-based coarse scan registration

3.1. Rough cylinder fitting to each scan

Fig. 2 gives an overview of the proposed cylinder-based registration and model fitting algorithm. The algorithm operates in three steps: rough cylinder fitting to each scanned point cloud, coarse registration, and fine registration.

In the first step, a set of cylindrical surfaces are detected in each scanned point cloud, each of which may represent a portion of a pipe. The axis position, orientation, and diameter of each is estimated using two different random sample consensus (RANSAC)-based algorithms: M-estimator Sample and Consensus (MSAC) [25] and efficient-RANSAC [19]. In MSAC, a set of hypothetical cylindrical surfaces are generated from a subset of point clouds sampled randomly from the scanned point clouds, and the hypothesis that best minimizes the sum of squared distances between the inlier points and the surface is chosen. In efficient-RANSAC, the hypotheses are generated by sampling a smaller subset of point clouds than that used in MSAC. This subset comprises locally-proximal points, making the random sampling process more efficient. As efficient-RANSAC requires point clouds with normal vectors, we applied PCA-based normal estimation to each point in the cloud. MSAC detects cylindrical surfaces more accurately than efficient-RANSAC, whereas efficient RANSAC is more efficient than MSAC. The algorithms were therefore alternated, reflecting the tradeoff between reliability and efficiency.

This rough cylinder fitting step is repeated until no more cylinders can be extracted. A set of the pairs (r_k^j, a_k^j) of radius r_k^j and with an axis a_k^j on the k-th cylindrical surface is extracted from j-th scan s^j, and these are used to find initial alignments among scans in the next step.

3.2. Coarse scan registration

In coarse scan registration, the best matches among cylinder axes are identified using a RANSAC-based method. This derives a rough initial alignment among all scans. The coarse registration process consists of the hash table generation and stochastic search for the best match among the cylinder axes.

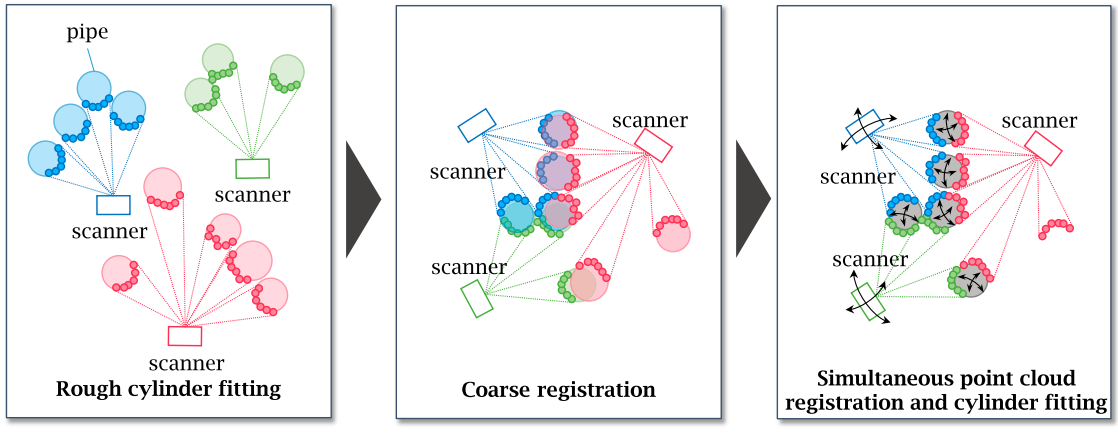

Figure 2. The proposed cylinder-based registration and model fitting algorithm.

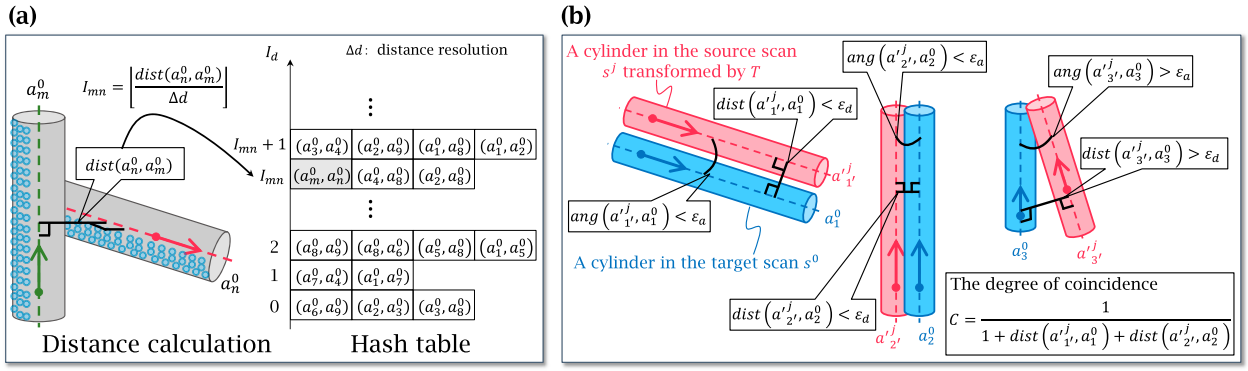

Figure 3. Coarse scan registration process: (a) Hash table generation, and (b) Evaluation of the degree of coincidence for a trans formation ***T***.

As shown in Fig. 3(a)., the hash table stores each pair of cylinder axes in one of the scans, which is treated as the *target scan* s^0. This is used to identify a corresponding pair of axes in the other scans, and can achieve matching to an original pair of axes, without performing an exhaustive search. To construct the hash table, every pair of non-parallel cylinder axes (a_n^0, a_m^0) in the target scan s^0 is chosen, and the distance $dist(a_n^0, a_m^0)$ between them is evaluated. This distance is then converted to an integer index I_{mn} by applying quantization $I_{mn} = \frac{dist(a_n^0, a_m^0)}{\Delta d}$, where Δd is a distance resolution. Finally, the axis pair (a_n^0, a_m^0) is stored at the entry indexed by I_{mn} in the table.

After the hash table has been constructed, a search for the best match among cylinder axes is performed, using the following steps:

(1) Two different scans are selected as the target scan s^0 and a source scan s^j.
(2) A pair of non-parallel cylinder axes $(a_{n'}^j, a_{m'}^j)$ is randomly selected from the source scan s^j, and the pair of axes (a_n^0, a_m^0) in s^0 with the closest distance to $dist(a_{n'}^j, a_{m'}^j)$ is retrieved from the hash table of s^0.
(3) A 3D transformation T for the source scan s^j is calculated, to align the non-parallel cylinder axes $(a_{n'}^j, a_{m'}^j)$ in the source scan s^j with (a_n^0, a_m^0) in the target scan s^0. The transformation T is applied to a set of all cylinder axes $A^j = \{a_l^j\}$ in the source scan s^j, to obtain a set of transformed source cylinder axes $A'^j = \{a'^j_l\}$.
(4) For each cylinder axis a_l^0 in the set of all cylinder axes A^0 in the target scan s^0, the coincident axis $a'^j_{l'}$ which satisfies $ang(a'^j_{l'}, a_l^0) < \varepsilon_a$ and $dist(a'^j_{l'}, a_l^0) < \varepsilon_d$ is picked up from the transformed axis set A'^j, if it exists. The angle threshold ε_a is set to 10°, while the distance threshold ε_d is set to half the minimum of the nominal outer pipe diameter (Φ10.5 mm), defined by the industry standards for plant piping systems [12].
(5) As shown in Fig. 3(b)., the degree of coincidence (i.e., consensus) C of this transformation T is given by $C = \left(1 + \sum_{a_l^0 \in A^0} dist(a'^j_{l'}, a_l^0)\right)^{-1}$.
(6) Steps 2) to 5) are iterated a specified number of times, and the transformation $\tilde{T}$ that gives the largest degree of coincidence between iterations is applied to the point clouds of the source scan s^j, generating a transformed source scan $\tilde{s}^j$.
(7) A union of scans s^0 U $\tilde{s}^j$ is generated, and this becomes the new target scan s^0. When taking the union, the cylinder axis retained is the one that has the greater number of inlier points between the two cylinders coincident to each other in s^0U $\tilde{s}^j$. Steps 2) to 6) are then repeated for the source scan s^j.

4. Cylinder-based fine scan registration based on simultaneous alignment and model fitting

4.1. Basic concept of fine scan registration

The proposed fine scan registration procedure minimizes the sum of the squared fitting errors at each point scanned from the corresponding exact cylindrical surface. The minimization procedure simultaneously adjusts the registration parameters (position and orientation) of the scanners and refines the model parameters (position, orientation, and radius) of the cylinders. This minimization is performed using Eqn. (4.1):

$$\min_{\{\boldsymbol{x}_j^{Reg}\}\{\boldsymbol{x}_k^{Cyl}\}} \sum_{j \in B-\{t_0\}} \sum_{k \in C} \sum_{i \in P_k} \left[D_{jk}(i; \boldsymbol{x}_j^{Reg}, \boldsymbol{x}_k^{Cyl})\right]^2 \qquad (4.1)$$

where, as shown in Fig. 4., B is a set of scanners, t_0 is a scanner at a reference (fixed) location, and C is a set of uniquely identified cylinders in all scans $\{s^j\}$. P_k

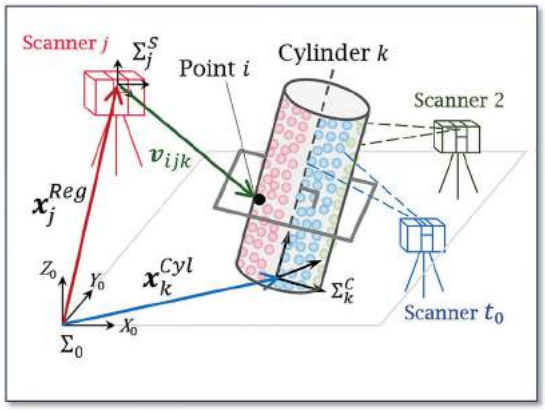

Figure 4. Fine scan registration.

denotes a set of scanned points placed on cylinder k, and $\boldsymbol{x}_k^{Cyl}$ are the model parameters of cylinder k. $\boldsymbol{x}_j^{Reg}$ denotes the registration parameters of scanner j. $D_{jk}(i;\boldsymbol{x}_j^{Reg},\boldsymbol{x}_k^{Cyl})$ denotes the signed fitting error function of a scanned point i from cylinder k located at $\boldsymbol{x}_k^{Cyl}$, when point i is captured by scanner j located at $\boldsymbol{x}_j^{Reg}$.

This simultaneous adjustment and refinement of $\boldsymbol{x}_j^{Reg}$ and $\boldsymbol{x}_k^{Cyl}$ prevents the alignment error of the fine registration from propagating to the following model fitting, and helps preserve the accuracy of the piping system model. Two fitting error functions are alternated for D_{jk},: the *orthogonal direction error* D_{jk}^o and the *beam direction error* D_{jk}^b. The modeling accuracy and the robustness of the adjustment depend on the function type. This is discussed in a later section.

4.2. Precise cylinder alignment by minimizing errors along an orthogonal direction

The orthogonal error function D_{jk}^o estimates the orthogonal distance of a point from its corresponding cylindrical surface. To simplify the calculation, we first classify the direction of the cylinder axis obtained from the course registration into one of the three dominant orthogonal axial directions (X_0, Y_0 or Z_0) in a world coordinate system Σ_0. This follows the self-calibration method used for scanners [4]. For example, as shown in Fig. 5(a)., when a cylinder axis is nearly parallel to the Z_0 axis, the error function D_{jk}^o is defined by Eqns. (4.2) and (4.3):

$$D_{jk}^o(i;\boldsymbol{x}_j^{Reg},\boldsymbol{x}_k^{Cyl}) = p_{ix}'^2 + p_{iy}'^2 - r_k^2 \tag{4.2}$$

$$\boldsymbol{p}_i' = \mathrm{R}(\Phi_k)\mathrm{R}(\Omega_k)\{\boldsymbol{p}_i - \boldsymbol{q}_k\} \tag{4.3}$$

where $\boldsymbol{p}_i = [p_{ix}, p_{iy}, p_{iz}]^t$ and $\boldsymbol{p}_i{}' = [p_{ix}', p_{iy}', p_{iz}']^t$ are the positions of a point i w.r.t. Σ_0 and a local coordinate system Σ_k^C fixed on cylinder k, with radius $r_k(\in \boldsymbol{x}_k^{Cyl})$, respectively. $\boldsymbol{q}_k = [q_{kx}, q_{ky}, 0]^t(\in \boldsymbol{x}_k^{Cyl})$ is the intersection point between the cylinder axis and the X_0Y_0 plane w.r.t. Σ_0, R() is a 3×3 rotation matrix, and Ω_k, Φ_k, $\Psi_k(\in \boldsymbol{x}_k^{Cyl})$ are the rotation angles about the X_0, Y_0, and Z_0 axes, respectively. These angles specify the axial orientation of cylinder k.

Similarly, when a cylinder axis is nearly parallel to the X_0 or Y_0 axis, the function D_{jk}^o is defined by Eqns. (4.4) and (4.5), or by Eqns. (4.6) and (4.7):

$$D_{jk}^o(i;\boldsymbol{x}_j^{Reg},\boldsymbol{x}_k^{Cyl}) = p_{iy}'^2 + p_{iz}'^2 - r_k^2 \tag{4.4}$$

$$\boldsymbol{p}_i' = \mathrm{R}(\Psi_k)\mathrm{R}(\Phi_k)\{\boldsymbol{p}_i - \boldsymbol{q}_k\} \tag{4.5}$$

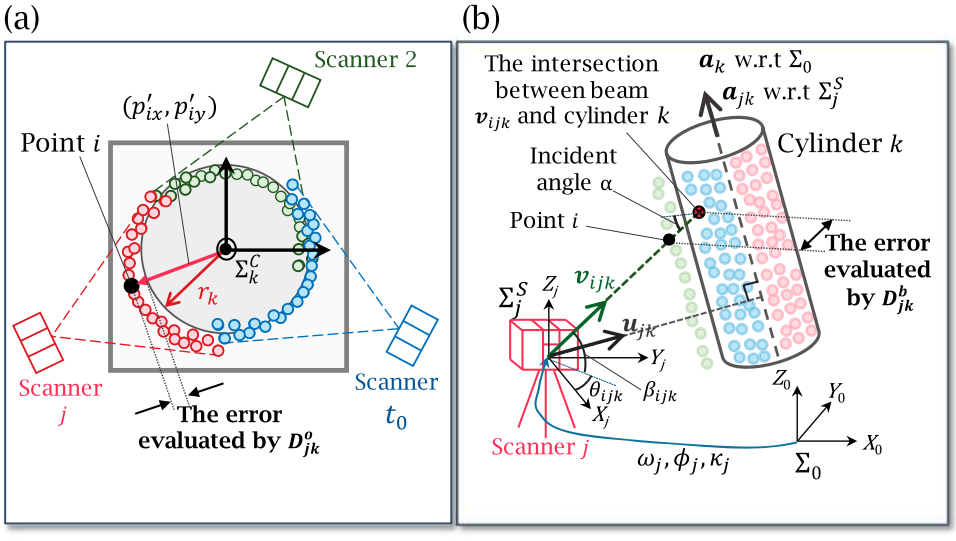

Figure 5. (a) Orthogonal error function and (b) beam direction error function.

Figure 6. Scanning of a PVC pipe by a TLS.

$$D^o_{jk}(i;\boldsymbol{x}_j^{Reg},\boldsymbol{x}_k^{Cyl}) = p'^2_{ix} + p'^2_{iz} - r_k^2 \tag{4.6}$$

$$\boldsymbol{p}'_i = \mathrm{R}(\Psi_k)\mathrm{R}(\Omega_k)\{\boldsymbol{p}_i - \boldsymbol{q}_k\} \tag{4.7}$$

4.3. Precise cylinder alignment by minimizing errors along beam direction

Strictly speaking, the accidental error of the scan follows a normal distribution along the beam incident direction at a scanned point. Therefore, as shown in Fig. 5(b)., the beam direction error function D^b_{jk} derives the distance of point i from its corresponding cylindrical surface k along the beam direction of the laser emitted by the scanner j, and the sum of errors at each point is minimized.

As shown in Fig. 5(b)., the beam direction error function D^b_{jk} is defined by Eqns. (4.8), (4.9), and (4.10).

$$D^b_{jk}(i;\boldsymbol{x}_j^{Reg},\boldsymbol{x}_k^{Cyl}) = \left(\lambda - \sqrt{\lambda^2 - \kappa\mu}\right)/\kappa - d_i \tag{4.8}$$

$$\kappa = 1 - (\boldsymbol{a}_{jk}\cdot\boldsymbol{v}_{ijk})^2,\ \lambda = \rho_{jk}(\boldsymbol{v}_{ijk}\cdot\boldsymbol{n}_{jk}),\ \mu = \rho_{jk}^2 - r_k^2 \tag{4.9}$$

$$\begin{aligned}\boldsymbol{a}_{jk} &= \mathrm{R}(\kappa_j)\mathrm{R}(\phi_j)\mathrm{R}(\omega_j)\boldsymbol{a}_k, \boldsymbol{n}_{jk} = \boldsymbol{u}'_{jk}/\rho_{jk}, \rho_{jk}\\ &= ||\boldsymbol{u}'_{jk}||, \boldsymbol{u}'_{jk} = \mathrm{R}(\kappa_j)\mathrm{R}(\phi_j)\mathrm{R}(\omega_j)\boldsymbol{u}_{jk}.\end{aligned} \tag{4.10}$$

Here, $\boldsymbol{a}_k$ and $\boldsymbol{a}_{jk}$ are the unit axis vectors of cylinder k w.r.t. Σ_0 and the local coordinate system Σ_j^S fixed at scanner j, respectively. The angles $\omega_j, \phi_j, \kappa_j (\in \boldsymbol{x}_j^{Reg})$ specify the orientations of the X_j, Y_j, and Z_j axes of Σ_j^S w.r.t. Σ_0. $\boldsymbol{v}_{ijk} = [\cos\beta_{ijk}\cos\theta_{ijk}, \cos\beta_{ijk}\sin\theta_{ijk}, \sin\beta_{ijk}]^t$ is the unit vector of the beam emitted by scanner j incident to point i on cylinder k, where θ_{ijk} denotes the azimuthal and β_{ijk} the elevation angle of the beam from scanner j w.r.t. Σ_j^S. $\boldsymbol{u}_{jk} = [u_{jkx}, u_{jky}, u_{jkz}]^t$ is the point position on the axis of the cylinder k that is closest to the origin of Σ_j^S w.r.t. Σ_0.

However, this error function D^b_{jk} becomes unstable as the beam incident angle approaches 90°, and the following special treatment is necessary. From Eqns. (4.8), (4.9), and (4.10), the cosine of the beam incidence angle α at the point of intersection between the beam and the estimated surface of cylinder k is given by Eqn. (4.11).

$$\cos\alpha = \sqrt{\lambda^2 - \kappa\mu}/r_k \tag{4.11}$$

If we specify that $\chi = \cos^2\alpha$, the beam is exactly tangent to the cylindrical surface when $\chi = 0$. Unfortunately, the error function D^b_{jk} has no real solution when $\chi < 0$, and moreover, the derivative function of Eqn. (4.8) diverges close to $\chi = 0$ as $\sqrt{\lambda^2 - \kappa\mu}$ approaches zero. Therefore, the beam direction error function D^b_{jk} must be modified to ensure the stability of calculation. This given by Eqn. (4.12):

$$\begin{aligned}&D^b_{jk}(i;\boldsymbol{x}_j^{Reg},\boldsymbol{x}_k^{Cyl})\\ &= \begin{cases}\left(\lambda - \sqrt{\lambda^2 - \kappa\mu}\right)/\kappa - d_i & (\chi > \varepsilon_c)\\ 0 & (otherwise)\end{cases}\end{aligned} \tag{4.12}$$

where ε_c is a threshold for the minimally allowable squared cosine of the beam incident angle. The derivative function of Eqn. (4.8) becomes unstable as the angle increases. The measurement results presented in Section 5 showed that the incident angle error increased abruptly from 60°. The threshold value ε_c was therefore set to $\cos^2 60^\circ$ in the experiments.

4.4. Optimization process

Applying the error functionD^o_{jk} from Eqns. (4.2), (4.4), and (4.6), or the D^b_{jk} of Eqn. (4.8) to D_{jk}, the minimization problem in Eqn. (4.1) must be solved for the registration parameters $\{\boldsymbol{x}_j^{Reg}\}$ and model parameters$\{\boldsymbol{x}_k^{Cyl}\}$. Because the error function D_{jk} represents a signed fitting error, and should become zero, the minimization in Eqn. (4.1) becomes a non-linear least squares problem. Moreover, from the coarse registration process described in Section 3, plausible initial guesses of the parameters $\boldsymbol{x}_j^{Reg}$ and $\boldsymbol{x}_k^{Cyl}$ are already available. Therefore, to find the solutions for the parameters $\{\boldsymbol{x}_j^{Reg}\}$ and $\{\boldsymbol{x}_k^{Cyl}\}$ for the minimization of Eqn. (4.1), we apply the Levenberg–Marquardt (LM) method [13]. The threshold for the convergence in the LM method is set to $\|\Delta\boldsymbol{X}\| < 10^{-6}$, where $\boldsymbol{X} = [\boldsymbol{x}_1^{Reg}|\boldsymbol{x}_2^{Reg}\ldots\ldots|\boldsymbol{x}_{|P_k|}^{Reg}|\boldsymbol{x}_1^{Cyl}|\boldsymbol{x}_2^{Cyl}\ldots\ldots|\boldsymbol{x}_{|C|}^{Cyl}]$.

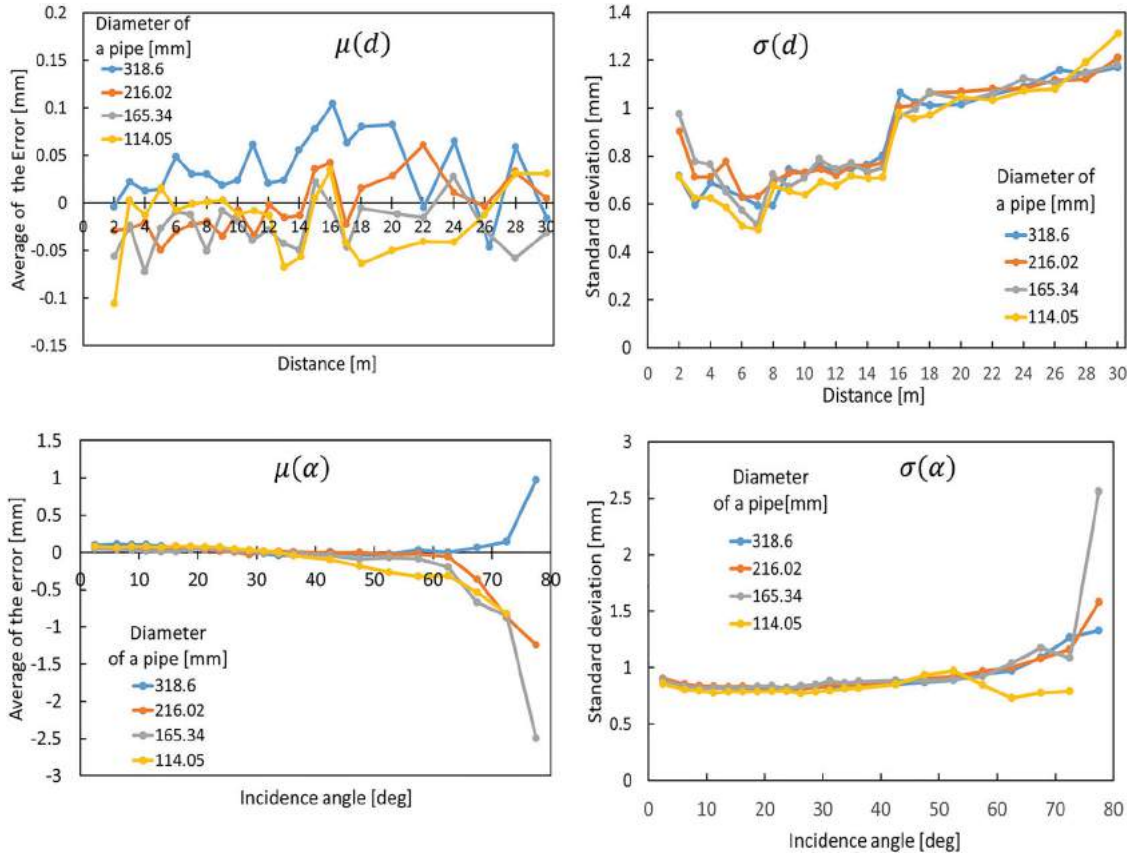

Figure 7. Average and standard deviation of cylinder measurement errors at different scan distances d and beam incident angles α. $\mu(d)$and $\sigma(d)$ are the average and deviation over all measured angles, and $\mu(\alpha)$and $\sigma(\alpha)$ are those over all measured distances.

The parameters $\{\boldsymbol{x}_j^{Reg}\}$ and $\{\boldsymbol{x}_k^{Cyl}\}$are further fine-tuned by one of two methods. The first filters out the set of scanned points from P_k in Eqn. (4.1) whose beam incident angle exceeds the threshold α_{th}. This method eliminates the large rise in accidental error at incident angles greater than 60° (see Fig. 7).

The second method assumes that the radius r_k should be identical to one of the standardized discrete pipe radii [12]. Therefore, once the optimum solutions to $\{\boldsymbol{x}_j^{Reg}\}$ and $\{\boldsymbol{x}_k^{Cyl}\}$ have been found in the first optimization, $r_k(\in \boldsymbol{x}_k^{Cyl})$ is replaced by this assumed radius $\widehat{r_k}$,and is thereafter treated as a constant. Finally, an additional convergence step is applied to the variable set $\{\boldsymbol{x}_k^{Cyl}\} - \{r_k\}$.

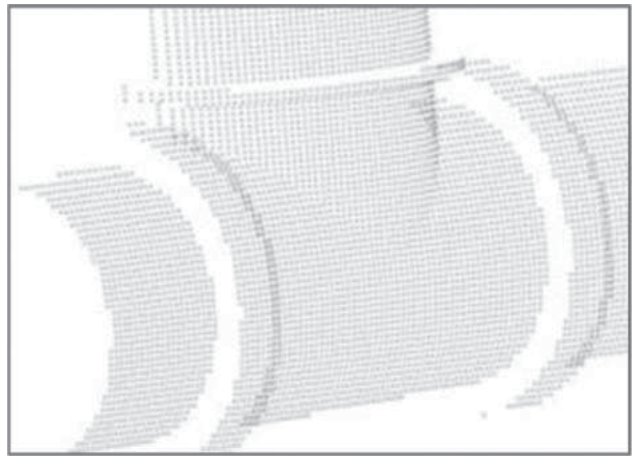

Figure 8. An example of point clouds generated by the scan simulation software (close-up).

5. Measurement error modeling and scan simulation

To allow the accuracy of registration and model fitting to be precisely determined, scan simulation software was developed in a preliminary study. This software generates laser-scanned point clouds in a 3D CAD model of a piping system, and superimposes artificial measurement errors onto them.

To determine the statistical distribution of the accidental errors, real pipes were measured using a TLS. As shown in Fig. 6., the surfaces of four PVC pipes with diameters ranging from Ø114.05 to Ø318.6 mm were covered with matt paper and captured by a TLS (FARO

Focus-3D-S120), at distances from 2 to 30 m. The optimal cylinder model was then fitted to the measured point clouds by the Levenberg–Marquardt method, and the deviation of each point from the fitted cylinder along the beam incident direction was treated as an error. The accidental errors were found to follow a normal distribution $\aleph(\mu(d,\alpha),\sigma^2(d,\alpha))$. As shown in Fig. 7., the average μ and standard deviation σ of the error depended on the scan distance d and the beam incident angle α. The functions $\mu(d,\alpha)$ and $\sigma^2(d,\alpha)$ take discrete values at a given interval $[d_l, d_{l+1}](\ni d), \alpha \in [\alpha_{l'}, \alpha_{l'+1}](\ni \alpha)$, centered at the measured values of d and α.

As shown in Fig. 7., the function $\sigma(d)$ decreased between 4 m and 12 m. This suggests that the TLS used in this experiment was in focus at a distance of approximately 7 m. The standard deviation σ also increased at a short range between 2 m and 6 m, and a long range between 16 m and 30 m. This was attributed to

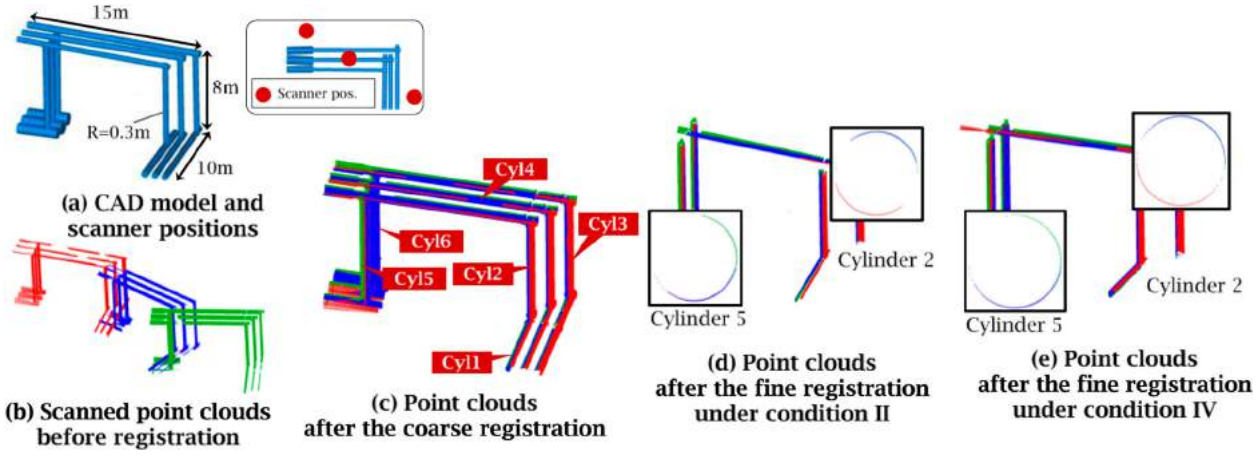

Figure 9. Results of coarse and fine registration for a simple piping system under condition II and IV.

Table 1. Fine registration conditions and convergence of the solution.

	Without incident angle filtering	With incident angle filtering
Orthogonal type error function	**Condition I** (Solution converged)	**Condition II** (Solution converged)
Beam direction type error function	(Solution is not converged)	**Condition III** (Solution converged)
Built-in ICP-based registration in commercial software	**Condition IV** (Cloud-Compare) **Condition V** (Geomagic) (Solution converged)	—

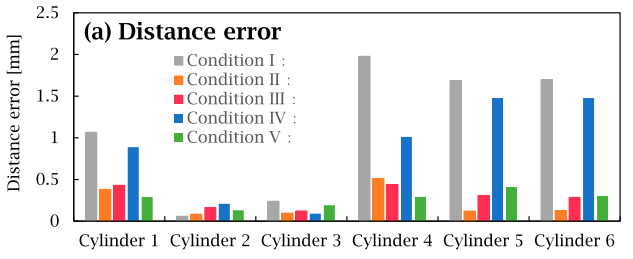

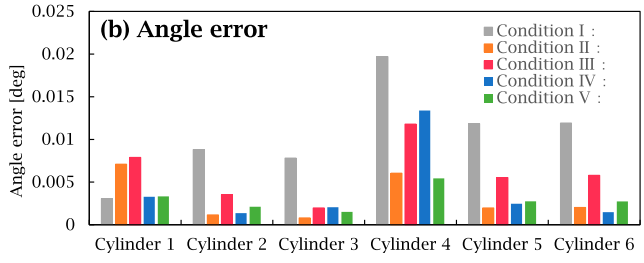

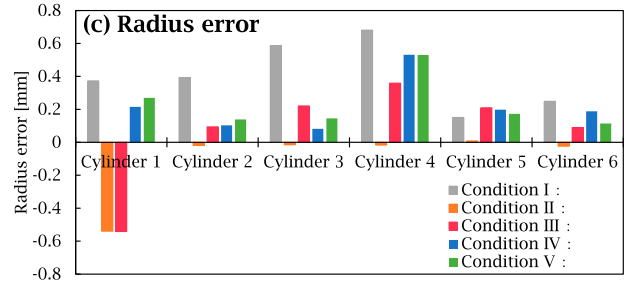

Average error	Distance error [mm]	Angle error [deg]	Radius error [mm]
Condition I	**1.12**	**0.011**	**0.41**
Condition II	**0.22**	**0.003**	**0.10**
Condition III	**0.29**	**0.006**	**0.25**
Condition IV	**0.86**	**0.004**	**0.22**
Condition V	**0.27**	**0.003**	**0.23**

(d) Average errors after fine registration

Figure 10. Error distribution of a simple piping system after fine registration under conditions I to V.

Table 2. Settings in scanned data and registration.

Scanned example	# of pipes	Method of scan	# of scans	Total # of scanned points	Rough cylinder fitting method	Incident angle filtering	Substation by standardized radius	Coarse registration time [min]	Fine registration time [min]
Simple piping system	15	Simulation	3	1.89M	MSAC [25]	Used & un-used	Used	0.02	1.0
Middle-scale piping system	≈ 100	Simulation	4	8.46M	MSAC [25]	Used & un-used	Used	2.0	8.0
Non overlapped point clouds	8	Simulation	3	1.61M	MSAC[25]	Used & un-used	Used	–	1.0
Real HVAC plant	≈ 50	Scanned by TLS	3	1.40M	Efficient-RANSAC [19]	Un-used	Un-used	1.5	1.0

CPU: Core i7-4930K/3.4GHz

an excessive detection of the reflected beam at short ranges, where the intensity is strong, and poor detection at long ranges, where it is weak. The functions $\mu(\alpha)$ and $\sigma(\alpha)$ increased rapidly at angles greater than 60°. That is because the footprint of the beam on surfaces becomes elliptical at large incident angles, significantly reducing the intensity of the reflected beam.

Based on the error model, the scan simulation software generated a set of artificial scanned points from the CAD model. A straight run of pipe was represented by a cylinder c, and the laser beam by a half line L. The scanned point $\boldsymbol{p}_i$ at which the error was to be superimposed was given by $\boldsymbol{p}_i = \boldsymbol{p}_i^e + \boldsymbol{l}\varepsilon(d,\alpha)$, where $\boldsymbol{p}_i^e$ denotes the exact intersection between c and L, $\boldsymbol{l}$ is a unit direction vector of the incident beam at $\boldsymbol{p}_i^e$, and $\varepsilon(d,\alpha)(\sim \aleph(\mu(d,\alpha),\sigma^2(d,\alpha)))$is the magnitude of the accidental error at $\boldsymbol{p}_i^e$. Fig. 8. gives a close-up view of one of the point clouds generated by the scan simulation software.

6. Evaluation of modeling and registration accuracy

6.1. Point clouds generated from the scan simulation for a simple piping system

In the first experiment, we compared the modeling and registration accuracy when the proposed method and conventional ICP-based methods were used, and investigated the effectiveness of filtering the point clouds from the beam incident angle. In a scan simulation, a CAD model of a simple piping system (10 m × 15 m × 8 m) comprising 15 straight pipes (Fig. 9(a).) was used, artificial scanned clouds with a total of 1.89 million points were captured from three scanner positions. These are shown in Fig. 9(b). These point clouds were processed first by the proposed coarse registration (Fig. 9(c).), using the MSAC cylinder fit, then by the simultaneous fine registration and model fitting, including the six manually-selected cylinders shown in Fig. 9(c).

To allow the accuracy to be compared, the fine registration was executed under four different conditions (see Tab. 1). Conditions I, II, and III differed in their error function type and incident angle filtering. In condition IV, fine registration was executed by the built-in ICP-based registration functions in the free software Cloud-Compare [5], and in condition V by the commercial software Geomagic-Wrap [8]. The cylinders were then individually fitted to the aligned point clouds using the Levenberg–Marquardt method. Panels (d) and (e) of Fig. 9 show the fine registration results under conditions II and IV, respectively.

The distance error between two cylinder axes is shown in Fig. 10(a), the angle error in Fig. 10(b), and the cylinder radius error in Fig. 10(c). The radius error was estimated for the radius values before substitution by standardized radii. As there exact values were derived directly from the CAD model, these errors could be evaluated.

As can be seen from Fig. 10(d)., the average errors of the proposed fine registration method were smaller under condition II (orthogonal error function D_{jk}^o with incident angle filtering) than under the other condition, including those using ICP-based methods. The distance and radius errors under condition II were less than 0.5 mm, which is well within the practical tolerances of a few millimeters required when aligning a piping system. Adopting the beam direction error function D_{jk}^b of condition III did not always reduce the errors generated from the case adopting the orthogonal error function D_{jk}^o of condition I and II. When adopting function D_{jk}^b without incident angle filtering, the minimization of Eqn. (4.1) sometimes failed to converge, and no solution appropriate for registration was found. As can be seen from Tab. 2., the total processing time under condition II was about 1 min.

In these cases, the proposed registration and modeling algorithm with incident angle filtering (condition II) was shown to have better accuracy than conventional ICP-based methods in deriving the position, orientation, and radii of the pipes, and the use of incident angle filtering was shown to increase the accuracy. Based on these preliminary results, the orthogonal error function D_{jk}^o (from conditions I and II) was used in the following experiments.

Moreover, the scan simulation software generated two additional artificial scanned point clouds which have more sparse and noisy points, and the fine registration under condition I was performed. In the sparse point clouds, the point-to-point interval at 10 m distance ranges approximately from 3 mm to 25 mm. While in case of the noisy point clouds, the accidental error magnitude ε in Section 5 was raised by 1.5 times. As a result, there was no significant change in the convergence was exhibited in the proposed method. Fig. 11 shows the registration accuracy for these clouds. The results changed at sub-millimeter level, but there was no significant reduction in accuracy.

6.2. Point clouds generated from a scan simulation of a mid-scale piping system

A second experiment was conducted to evaluate the modeling and registration accuracy when using scanned point clouds to represent a more complex and realistic

(a)

Point-to-point interval @10m	Distance error [mm]	Angle error [deg]	Radius error [mm]
3.1 mm	0.389	0.017	0.46
6.1 mm	0.385	0.021	0.49
7.7 mm	0.334	0.017	0.40
12.3 mm	0.282	0.018	0.33
15.3 mm	0.245	0.022	0.23
24.5 mm	0.401	0.019	0.41

(b)

The accidental error magnitude	Distance error [mm]	Angle error [deg]	Radius error [mm]
×1.0	0.385	0.021	0.49
×1.5	0.424	0.022	0.36

Figure 11. Error distribution of a simple piping system after fine registration under conditions I on sparse and noisy dataset: (a) Average errors after fine registration with more sparse points, and (b) Average errors after fine registration with noisy points.

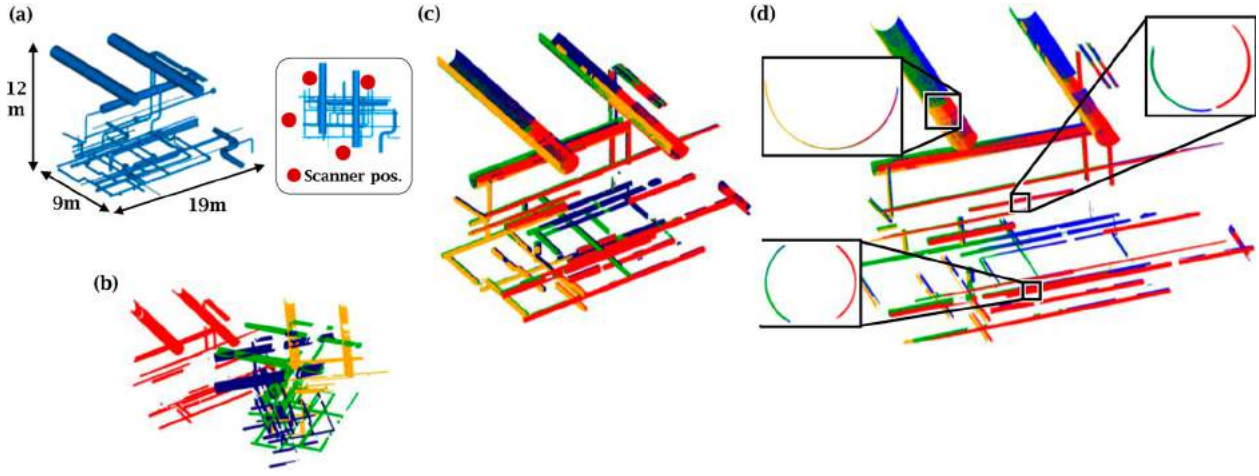

Figure 12. Results of coarse and fine registration for a mid-scale piping system under condition II: (a) CAD model of a chemical plant piping system, (b) Scanned point clouds before registration, (c) Coarse registration result under condition II, and (d) Fine registration result under condition II.

piping system, and to investigate the effectiveness of incident angle filtering. A scan simulation generated artificial scanned point clouds from four scanner positions in a CAD model of a real mid-scale chemical plant piping system (19 m × 9 m × 12 m), as shown in Fig. 12(a). The clouds, shown in Fig. 12(b) contained a total of 8.46 million points representing approximately one hundred straight pipes. In the rough cylinder fitting, MSAC identified fifty to seventy cylinders in each scan. Figs. 12(c) and (d) show the aligned point clouds under condition II, after coarse and fine registration, respectively.

The distance error between two cylinder axes is shown in Fig. 13(a) the angle error in Fig. 13(b)., and the cylinder radius error in Fig. 13(c)., after fine registration under conditions I and II. Under condition II, the distance, angle, and radius errors averaged 0.35 mm, 0.0196°, and 0.22 mm, respectively. These values were sufficiently small, and the accuracy of the as-built modeling of the pipes was confirmed. However, the incident angle filtering was found to have no significant effect. The total processing time under condition II was approximately 10 min.

6.3. Non-overlapped point clouds from the scan simulation

In a third experiment, the proposed method (conditions I and II) and two conventional ICP-based methods (conditions IV and V) were applied to the critical case in which there is no overlap between three scanned point clouds. Clouds with a total of 1.6 million points were generated for a system of eight pipes (16 m × 4 m × 8 m) using scan simulations. The results are shown in Fig. 14(a).

Figs. 14(b) and (c) show that the proposed fine registration (conditions I and II) was successful, and that the distance and radius errors remained within an acceptable sub-millimeter range. In contrast, the fine registration of the free and commercial software (conditions IV and V) failed completely, as can be seen from Figs. 14(d) and (e). The results demonstrated that the proposed registration

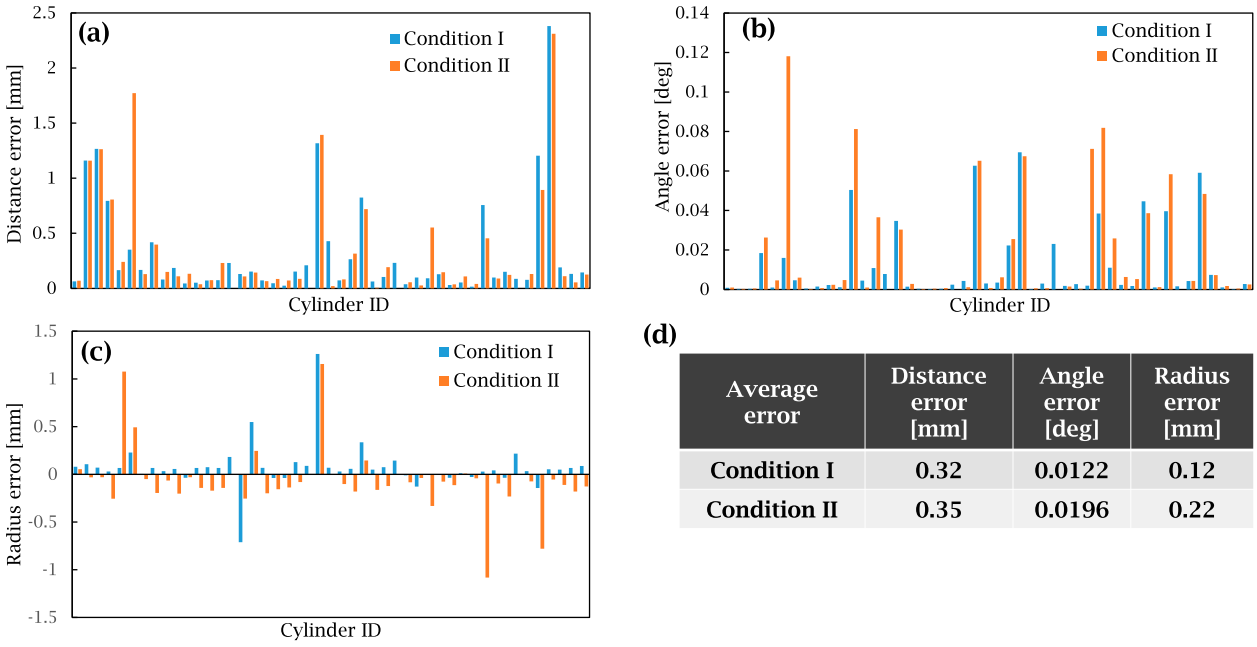

(d)

Average error	Distance error [mm]	Angle error [deg]	Radius error [mm]
Condition I	0.32	0.0122	0.12
Condition II	0.35	0.0196	0.22

Figure 13. Error distribution for a mid-scale piping system under conditions I and II: (a) Distance error, (b) Angle error, (c) Radius error, and (d) Average errors after fine registration.

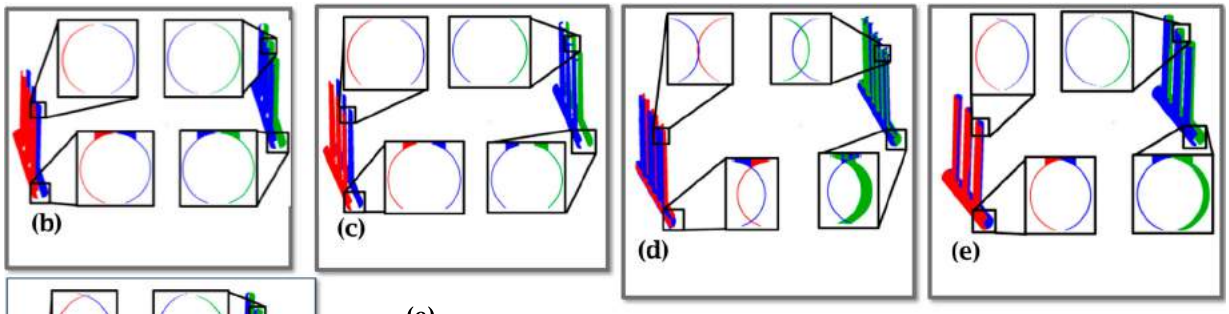

(e)

Average error	Distance error [mm]	Angle error [deg]	Radius error [mm]
Condition I	0.007	0.003	0.14
Condition II	0.010	0.004	0.22

Average errors after fine registration under condition I and II

Figure 14. Results of coarse and fine registration for non-overlapped scans: (a) Point clouds after the coarse registration, (b) Fine registration under condition I, (c) Fine registration under condition II, (d) Fine registration under condition IV, (e) Fine registration under condition V, and (f) Average errors after fine registration under condition I and II.

method provided robust modeling and accurate registration of the piping system.

6.4. Real point clouds for a piping system of an HVAC plant

Finally, the proposed modeling and registration methods were applied under condition I to scanned point clouds captured from the real piping system (20 m × 15 m × 8 m) of an urban HVAC plant. Data were captured using a TLS (Leica, HDS7000). As shown in Fig. 15(a) the point clouds were taken from three scans, with a total of 1.4 million points. Background point clouds from walls, floors, ceilings, and facilities other than piping were removed manually, before applying efficient-RANSAC [19] to the rough cylinder fitting to speed up the coarse scan registration. Figs. 15(b) and (c) show the results of the coarse and fine registration, respectively.

Because no reference CAD model of this plant was available, we were only able to evaluate the distribution

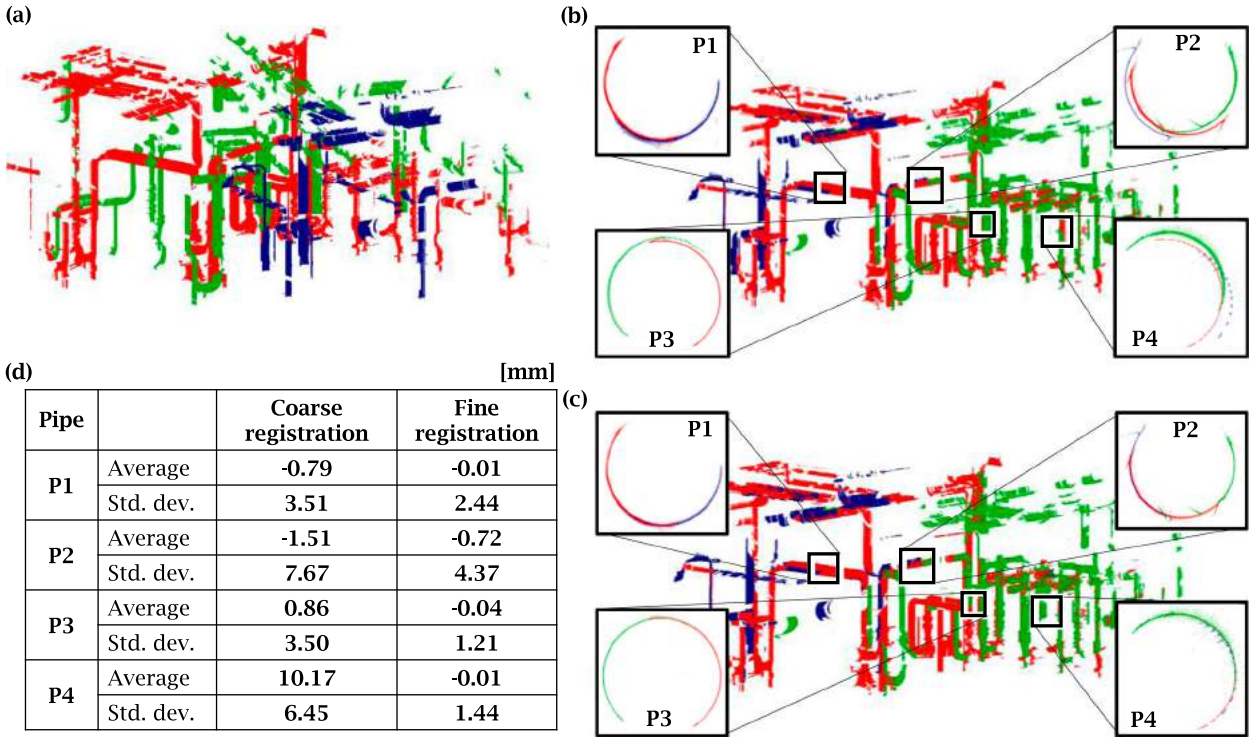

(d) [mm]

Pipe		Coarse registration	Fine registration
P1	Average	-0.79	-0.01
	Std. dev.	3.51	2.44
P2	Average	-1.51	-0.72
	Std. dev.	7.67	4.37
P3	Average	0.86	-0.04
	Std. dev.	3.50	1.21
P4	Average	10.17	-0.01
	Std. dev.	6.45	1.44

Figure 15. Results of coarse and fine registration for an HVAC plant and reduction in the radius errors: (a) Scanned point clouds before registration, (b) Coarse registration result under condition I, (c) Fine registration result under condition I, and (d) Distributions of the radius errors at four sampled pipes (P1 ∼ P4) in coarse and fine registration.

of radius errors before and after fine registration from the cylindrical surfaces. These were best fitted to the point clouds of each pipe using the Levenberg–Marquardt method. Coarse registration was completed in 1.5 min, and fine registration in 1 min.

As can be seen from Fig. 15(d) the deviation among the three scans and the distribution of radius errors for four sampled pipes decreased after the proposed fine registration was applied. The average errors were at the sub-millimeter level for all sampled pipes. The standard deviations also reduced, despite the presence of a good number of outlier points near the surface, as shown in Fig. 15(c). This confirmed that the proposed modeling and registration method worked well when applied to real laser-scanned point clouds, and that the accuracy of as-built modeling was within a range acceptable for use in practical applications.

7. Conclusions

In this study, we proposed a novel algorithm for registration and model fitting of laser-scanned point clouds. The algorithm was specifically designed for as-built modeling of the cylindrical pipe systems of HVAC plants. Coarse registration was automated by applying a rough cylinder fit to the scans and using a RANSAC-based process. In contrast with conventional ICP-based methods, fine registration and cylinder model fitting were performed simultaneously, by solving a nonlinear equation. In simulations, the proposed algorithm outperformed conventional ICP-based registration in both accuracy and robustness against zero scan overlap. Our approach was then applied to point clouds scanned from a real HVAC plant, with successful results. The proposed algorithm was demonstrated to achieve as-built modeling accuracies that would be fully acceptable when conducting renovation work on existing piping systems.

In future work, the precision of registration will be improved by introducing a weighted least-squares solution, based on the measuring error estimated at a scanned point. It may also be possible to obtain better modeling accuracy by integrating the proposed registration with self-calibration of systematic mechanical errors from a laser scanner using cylinders [4].

ORCID

Ryota Moritani http://orcid.org/0000-0001-5051-7890
Satoshi Kanai http://orcid.org/0000-0003-3570-1782
Hiroaki Date http://orcid.org/0000-0002-6189-2044
Masahiro Watanabe http://orcid.org/0000-0003-2486-7648
Takahiro Nakano http://orcid.org/0000-0002-6946-5629
Yuta Yamauchi http://orcid.org/0000-0003-0289-8398

References

[1] Al-Durgham, M.; Detchev, I.; Habib, A.: Analysis of two triangle-based multi-surface registration algorithms of irregular point clouds, *ISPRS Int. Arch. Photogramm. Remote Sens. Spat. Inf. Sci.*, XXXVIII-5/W12, 2011, 61–66. https://doi.org/10.5194/isprsarchives-XXXVIII-5-W12-61-2011

[2] Al-Durgham, K.; Habib, A.; Kwak, E.: RANSAC approach for automated registration of terrestrial laser scans using linear features, ISPRS Ann. *Photogramm. Remote Sens. Spatial Inf. Sci.*, II-5/W2, 2013, 13–18. https://doi.org/10.5194/isprsannals-II-5-W2-13-2013

[3] Besl, P.J.; McKay, N.D.: A method for registration of 3-D shapes, *IEEE Trans. on Pattern Analysis and Machine Intelligence,* 142), 1992, 239–256. https://doi.org/10.1109/34.121791

[4] Chan, T.O.; Lichti, D.D.; Belton, D.: A rigorous cylinder-based self-calibration approach for terrestrial laser scanners, *ISPRS Journal of Photogrammetry and Remote Sensing*, 99, 2015, 84–99. https://doi.org/10.1016/j.isprsjprs.2014.11.003

[5] Cloud-Compare. https://www.danielgm.net/cc/

[6] Fischler, M.A.; Bolles, R.C.: Random Sample Consensus: A paradigm for model fitting with applications to image analysis and automated cartography, *Comm. of the ACM,* 24(6), 1981, 381–395. https://doi.org/10.1145/358669.358692

[7] Ge, X.; Wunderlich, T.: Surface-based matching of 3D point clouds with variable coordinates in source and target system, *ISPRS Journal of Photogrammetry and Remote Sensing,* 111(1), 2016, 1–12. https://doi.org/10.1016/j.isprsjprs.2015.11.001

[8] Geomagic-Wrap, https://www.geomagic.com/en/products/wrap/overview, 3D systems.

[9] Gruen, A.; Akca, D.: Least squares 3D surface and curve matching, *ISPRS Journal of Photogrammetry and Remote Sensing,* 59(3), 2005, 151–174. https://doi.org/10.1016/j.isprsjprs.2005.02.006

[10] Habib, A.; Mwafag, G.; Michel, M.; Al-Ruzouq, R.: Photogrammetric and LIDAR data registration using linear features, *Photogrammetric Engineering & Remote Sensing,* 71(6), 2005, 699–707. https://doi.org/10.14358/PERS.71.6.699

[11] Habib, A.; Detchev, I.; Bang, K.: A comparative analysis of two approaches for multiple-surface registration of irregular point clouds, *ISPRS Int. Arch. Photogramm. Remote Sens. Spat. Inf. Sci.*, XXXVIII-1, 2010, 61–66. https://www.isprs.org/proceedings/XXXVIII/part1/03/03_03_Paper_39.pdf

[12] JIS G3452:2014, Carbon steel pipes for ordinary piping. https://www.webstore.jsa.or.jp/webstore/top/index.jsp

[13] Marquardt, D.: An Algorithm for Least-Squares Estimation of Nonlinear Parameters, *SIAM Journal on Applied Mathematics,* 11(2), 1963, 431–441. https://doi.org/10.1137/0111030

[14] Pomerleau, F; Colas, F.; Siegwart, R.; Magnenat, S.: Comparing ICP variants on real-world data sets, *Autonomous Robots,* 34(3), 2013, 133–148. https://doi.org/10.1007/s10514-013-9327-2

[15] Previtali, M.; Barazzetti, L.; Brumana, R.; Scaioni, M.: Laser scan registration using planar features, *Int. Arch. Photogramm. Remote Sens. Spatial Inf. Sci.*, XL-5, 2014, 501–508. https://doi.org/10.5194/isprsarchives-XL-5-501-2014

[16] Pulli, K.: Multiview registration for large data sets, Second international conference on 3-D Digital imaging and modeling, 1999, 160–168. https://doi.org/10.1109/IM.1999.805346

[17] Rusinkiewicz, S.; Levoy, M.: Efficient variants of the ICP algorithm, Proceedings 3rd International Conference on 3-D Digital Imaging and Modeling, 2001, 145–152. https://doi.org/10.1109/IM.2001.924423

[18] Rusu, R.B.; Blodow, N.; Beetz, M.: Fast point feature histograms (FPFH) for 3D registration, Proceedings of IEEE International Conference on Robotics and Automation, 2009, 3212–3217. https://dl.acm.org/citation.cfm?id=1703435.1703733

[19] Schnabel, R.; Wahl, R.; Klein, R.: Efficient RANSAC for point-cloud shape detection, *Computer Graphics Forum,* 26(2), 2007, 1467–8659. https://doi.org/10.1111/j.1467-8659.2007.01016.x

[20] Stamos, I.; Leordeanu, M.: Automated feature-based range registration of urban scenes of large scale, *Proceedings of IEEE Computer Society Conference on Computer Vision and Pattern Recognition*, 2, 2003, 555–56. https://doi.org/10.1109/CVPR.2003.1211516

[21] Tam, G.K.L.et al.: Registration of 3D point clouds and meshes: A survey from rigid to nonrigid, *IEEE Trans. on Visualization and Computer Graphics,* 19(7), 2013, 1199–1217. https://doi.org/10.1109/TVCG.2012.310

[22] Thapa, A.; Pu, S.; Gerke, M.: Semantic feature based registration of terrestrial point clouds, *Proceedings of Laser scanning 2009, ISPRS*, Vol. XXXVIII, Part 3/W8, 2009, 230-235. www.isprs.org/proceedings/XXXVIII/3-W8/papers/p87.pdf

[23] Theiler, P. W.; Schindler, K.: Automatic Registration of Terrestrial Laser Scanner Point Clouds Using Natural Planar Surfaces, *ISPRS Ann. Photogramm. Remote Sens. Spatial Inf. Sci.*, I-3, 2012, 173–178. https://doi.org/10.5194/isprsannals-I-3-173-2012

[24] Theiler, P.W., Wegner, J.D., Schindler, K.: Keypoint-based 4-points congruent sets – Automated marker-less registration of laser scans, *ISPRS Journal of Photogrammetry and Remote Sensing*, 96, 2014, 149–163. https://doi.org/10.1016/j.isprsjprs.2014.06.015

[25] Torr, P.H.S.; Zisserman, A.: MLESAC: A new robust estimator with application to estimating image geometry, *Computer Vision and Image Understanding,* 78(1), 2000, 138–156. https://doi.org/10.1006/cviu.1999.0832

[26] Weinmann, M.; Jutzi, B.: Geometric point quality assessment for the automated, markerless and robust registration of unordered TLS point clouds, *ISPRS Ann. Photogramm. Remote Sens. Spatial Inf. Sci.*, II-3/W5, 2015, 89–96. https://doi.org/10.5194/isprsannals-II-3-W5-89-2015

[27] Yang, B.; Dong, Z.; Liang, F.; Liu, Y.: Automatic registration of large-scale urban scene point clouds based on semantic feature points, *ISPRS Journal of Photogrammetry and Remote Sensing*, 113, 2016, 43–58. https://doi.org/10.1016/j.isprsjprs.2015.12.005

[28] Zhang, M.: Accurate sphere marker-based registration system of 3D point cloud data in applications of shipbuilding blocks, *Journal of Industrial and Intelligent Information,* 3(4), 2015, 318–323. https://doi.org/10.12720/jiii.3.4.318-323